Available online at www.sciencedirect.com
ScienceDirect
International Journal of Heat and Fluid Flow 28 (2007) 329–339
International Journal of HEAT AND FLUID FLOW
www.elsevier.com/locate/ijhff

A thermal periodic boundary condition for heating and cooling processes

S.A. Mohsen Karimian, Anthony G. Straatman *

The University of Western Ontario, Department of Mechanical and Materials Engineering, London, Ont., Canada N6A 5B9

Received 3 January 2006; received in revised form 27 March 2006; accepted 30 March 2006
Available online 14 June 2006

Abstract

A thermal periodic boundary condition is developed to compute heat transfer in spatially periodic domains. The condition is formulated on the basis of thermal similarity and is implemented within the framework of a mass flow-based periodic condition for the flow field. The thermal periodic boundary condition is validated by computing the flow and heat transfer for fully developed pipe flow under constant heat flux and constant wall temperature conditions, and for a generic spatially periodic geometry.

Keywords: Periodic boundary condition; Convective heat transfer; Finite-volume method; Unstructured grid

1. Introduction

Flow in arbitrary-shaped spatially periodic geometries occurs in many fluid dynamics and heat transfer applications, e.g. turbomachines, heat exchangers and porous media. A periodic or representative cell, subsequently referred to as cell, is an element that is spatially repeated to form the periodic geometry. The structure of the fully developed flow field inside each cell is identical. The repeating behavior of the flow is the basic element in defining periodic boundary conditions in computational fluid dynamics (CFD) problems. When heating or cooling occurs, the thermal characteristics of the fully developed flow based on temperature do not repeat for each cell. However, when a constant temperature or constant heat flux is imposed at the walls, the nature of the thermal process is similar for all cells. Quantifying this similarity is important for developing an accurate and realistic periodic boundary condition for the energy equation.

Periodic boundary conditions are used to truncate the computational domain by taking advantage of periodicity in the structure of the flow or similarity in the boundary conditions defining the problem. There are different ways of defining periodic boundary conditions. However, one rule is common among all of them: that the periodic boundaries *must* be transparent. The boundaries must be invisible to the flow domain. Therefore, periodic boundary conditions should be defined in a way that the real similarities are kept in the domain and the numerical errors are expelled out of the domain. Two different types of periodic boundary conditions for fluid flow are recognized: pressure gradient-specified and mass flow-specified boundary conditions. In the pressure-gradient method, the outflow boundary is *virtually* attached to the inflow boundary and hence, the mass and momentum fluxes are conserved through the periodic boundaries. The numerical errors, however, also pass through the periodic boundaries. Moreover, in this method, the momentum flux exiting from the outlet of each cell directly enters the inlet of that cell, whereas in reality, due to the presence of wall shear forces, the outlet momentum flux is lower than that of the inlet. To compensate the loss of momentum and to drive the flow, a constant streamwise pressure gradient is imposed as a source of momentum

* Corresponding author. Tel.: +1 519 661 2111x88249; fax: +1 519 661 3020.
E-mail addresses: skarimia@uwo.ca (S.A. Mohsen Karimian), astraatman@eng.uwo.ca (A.G. Straatman).

0142-727X/$ - see front matter © 2006 Elsevier Inc. All rights reserved.
doi:10.1016/j.ijheatfluidflow.2006.03.023

over the computational domain. There are two drawbacks with this technique: First, in many cases including turbulent flow and flow in geometries with periodically varying shapes, imposition of a constant pressure gradient is not physically realistic. In some cases, decomposition of the pressure field into two pressure fields, one with constant streamwise gradient and one with periodic behavior, alleviates the problem (Patankar et al., 1977), while in other cases, e.g. turbulent flows, more elaborate techniques must be implemented to guarantee physical results (Orlandi, 2000). Second, the mass flow rate is a result of the computation and if results are required for a particular mass flow rate, implementation of this type of condition requires an iterative computation by varying the pressure gradient until the desired mass flow rate is achieved. A mass flow-specified method was recently developed by El Soukkary and Straatman (2003) to predict the flow in spatially periodic geometries. This method is based on the double-periodic-cell configuration suggested by Nicolas et al. (1997). In this method, a specified mass flow rate is conserved by taking the velocity pattern from the outlet and imposing it to the inlet with a correction to meet the target mass flow rate. Any numerical error causing an increase or decrease in mass flow is washed out of the computational domain. Using this condition, a proper pressure boundary condition is imposed at the outlet and the pressure everywhere else, including the inlet, is determined by solving the mass and momentum equations and hence, the pressure drop emerges as part of the solution. Thus, the momentum evolves in the computational domain without any non-physical restriction. In cases where the mass flow rate is known or a constant pressure gradient along the streamwise direction is not known, the mass flow specified method is more desirable.

Both methods outlined above are formulated based on the identical structure of the fully developed flow field in a periodic geometry. The fully developed temperature field, however, is not identical in each cell. When heating or cooling occurs at the walls, the amount of heat convected by the flow increases/decreases in the streamwise direction. Therefore, attaching the outlet to the inlet, as suggested by the pressure-gradient method for the flow field, and conserving the heat flux through the periodic boundaries will not simulate a fully developed temperature field in a fixed section of a periodic geometry. Using a scaled temperature profile with the mass-based approach will only yield a physical result if the scaling law is defined based on the thermal process and a variation in the temperature profile in streamwise direction is considered. It can be shown from Incropera and DeWitt (2002) that the thermal behavior of the flow in an arbitrary shaped duct is a function of the geometry and the wall temperature. Therefore, the nature of the thermal behavior of the flow is similar for each cell of a periodic geometry with constant wall temperature or constant wall heat flux. A reasonable condition is the one that establishes this similarity.

Two separate methods were proposed by Patankar et al. (1977) for thermal periodic boundary conditions to be used in conjunction with the pressure-gradient specified boundary conditions: one method for constant wall heat flux and one method for constant wall temperature boundary conditions. In both methods, a similar technique to that implemented for the pressure field is adopted, wherein the temperature field is decomposed into a periodic component (temperature-perturbation field) and a variable component (mean/bulk temperature field) which is a function of the streamwise direction. The energy equation is then solved for the periodic component with an additional source term to compensate the heat addition/removal at the walls. For the case of constant wall heat flux, the non-periodic component is a constant temperature gradient, which is a function of geometry, wall heat flux and mass flow rate, and which must be computed *a priori*. For the case of constant wall temperature, the additional source term is a function of bulk temperature, and must, therefore, be computed by solving an additional set of partial differential equations integrated over axial cross-sections. In both cases, the complete temperature field is computed by super-imposing its periodic and non-periodic components. Aside from the difficulties and computational costs raised by the additional set of partial differential equations in the case of constant wall temperature, the implementation of two completely different methods with different energy equations complicates a numerical code. Furthermore, the method developed for the isothermal condition also requires integration in the cross-stream direction. Though this is a straightforward process in a structured grid, it is quite difficult to develop such a process for unstructured grids that are decomposed among distributed memory machines in a parallel computing environment. All these points suggest that it is desirable to develop a method for imposing thermal periodic boundary conditions that is suitable for both wall thermal conditions considered and is easy to implement on structured or unstructured grids.

In the present work, a periodic thermal boundary condition is developed. This boundary condition is based on the same geometric configuration as that used by El Soukkary and Straatman (2003). The condition is developed such that it complies with the thermal similarity found in a fully developed thermo-fluid flow. The method is suitable and consistent for both isothermal and isoflux wall conditions and is easy to implement on all kinds of grids. Using this method, the energy equation is solved for the primitive variable, i.e. temperature, and there are no additional partial differential equations to solve. The periodic thermal boundary condition is validated by computing the heat transfer (and pressure drop) for fully developed pipe flow under isothermal and isoflux conditions and comparing the results to the exact analytical solutions. The utility of the thermal boundary condition is then demonstrated by computing the flow and heat transfer through an idealized section of a porous material. In the following sections the governing equations and the numerical method are described briefly

followed by the development of the method for periodic boundary condition and the validation.

2. Governing equations and numerical method

Consider an arbitrary fixed control volume $\Omega \subset R^3$, of volume V and a piecewise smooth boundary $\partial\Omega$, with unit normal surface vector $\hat{n}$ pointing outwards, occupied by an incompressible, Newtonian fluid. The integral form of the conservation equations for mass, momentum and energy is given by

$$\int_{\partial\Omega} \rho \vec{V} \cdot \hat{n}\, \mathrm{d}s = 0, \tag{1}$$

$$\int_{\Omega} \rho \partial_t \vec{V}\, \mathrm{d}v + \int_{\partial\Omega} \hat{n} \cdot (\rho \vec{V}\vec{V})\, \mathrm{d}s - \int_{\partial\Omega} \hat{n} \cdot (\mu \nabla \vec{V})\, \mathrm{d}s = -\int_{\partial\Omega} P\hat{n}\, \mathrm{d}s, \tag{2}$$

$$\int_{\Omega} \rho \partial_t T\, \mathrm{d}v + \int_{\partial\Omega} \hat{n} \cdot (\rho \vec{V} T)\, \mathrm{d}s - \int_{\partial\Omega} \hat{n} \cdot \left(\frac{k}{c_p} \nabla T\right) \mathrm{d}s = 0, \tag{3}$$

where ρ is the density, μ is the viscosity, k is the heat conductivity coefficient, c_p is the specific heat, p is the relative pressure, $\vec{V}$ is the velocity vector, T is the absolute temperature, $\mathrm{d}s$ is the surface differential and $\mathrm{d}v$ is the volume differential.

The parallel code (ParTISUN) developed by Karimian and Straatman (in press) is used to discretize and solve Eqs. (1)–(3) using an implicit, unstructured finite-volume method. A single-program-multiple-data (SPMD) parallelization model was implemented in the code within the PETSc framework (Balay et al., 2001) to exploit the maximum capability of a cluster of distributed-memory machines. An inexact Jacobian Newton–Krylov (iJNK) method was used in conjunction with the non-linear iterations to accelerate the non-linear convergence in each time-step. The convection term is implicitly modeled using a first-order upstream difference scheme (UDS) and explicitly corrected to higher-order using a deferred-correction technique (Kholsa and Rubin, 1974). In this work, a second-order central difference scheme is selected as a higher-order scheme. However, there is no limit in using other higher-order schemes. The details of the discretization method, parallel implementation and iJNK technique may be found in Karimian and Straatman (in press) and are omitted here for brevity.

3. Periodic boundary conditions

Consider a geometry with a periodically repeating pattern in the streamwise direction, an example of which is shown in Fig. 1(a). This type of spatially periodic geometry occurs in a wide range of applications, from simple pipes to the micro-structure of porous media. A generalized definition of a fully developed flow in such periodic geometries is a flow whose structure is identical in each cell. Using this definition, a periodic boundary condition for the flow field can be easily defined using either of the methods outlined in Section 1. In occurrence of heat transfer at the walls, the temperature field is not identical in each cell. Therefore, developing a thermal periodic boundary condition requires a better understanding of the heat transfer process and a definition of similarity in the temperature field.

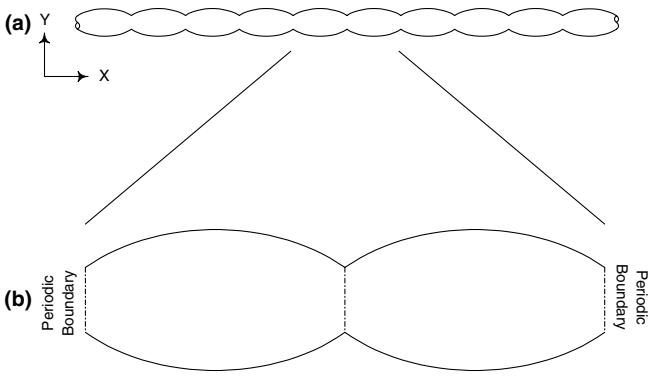

Fig. 1. (a) Schematic of a pipe with periodically varying diameter and (b) its representative double-periodic-cell, an example of spatially periodic geometries.

3.1. Flow periodic boundary condition

The rationale behind the method implemented herein is similar to that of El Soukkary and Straatman (2003). A double-periodic-cell geometry configuration is used, which reduces the computational domain to two consecutive spatially periodic cells. Fig. 1(b) shows a double-periodic-cell for the geometry shown in Fig. 1(a). Based on the definition of a periodic cell, each cell starts with one periodic section and ends with another periodic section. Information is transferred iteratively from one periodic section to another as boundary conditions, until a fully developed flow field evolves. Therefore, to have a complete and self-sustained computational method, one or more source(s) of information is required. There are three periodic sections in a double-periodic-cell (see Fig. 2): Section 1, where the inflow periodic boundary condition is imposed, Section 3, where the outflow periodic boundary condition is imposed and Section 2, which is in the middle of the computational domain and is periodic with the other two sections. The best choice for the source of information is Section 2 because the quantities at Section 2 are evaluated by interpolation at the middle of the computational domain where the flow field is not directly influenced by boundary conditions. Ideally, for a fully developed flow, the velocity profile at the outlet of each cell is the same as the velocity profile at the inlet of that cell. However, due to inaccuracies in the pressure field and because of the implementation of an iJNK method, the continuity equation is not solved accurately in the beginning of each time-step. This introduces errors in the mass flow. By copying the velocity profile from Section 2 directly to the inlet boundary, the errors

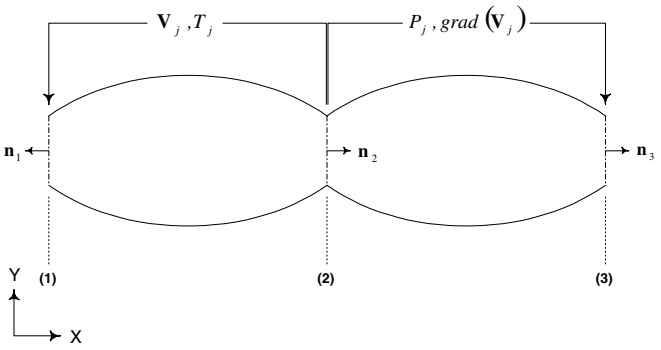

Fig. 2. Schematic showing two periodic cells and the imposition of periodic boundary conditions and the transfer of the information.

in the mass flow are carried to the next iteration, potentially leading to a change in the mass flow rate. To remedy this problem, the velocity profile is taken node-by-node from Section 2 and then modified to meet the target mass flow rate using the following correction technique before it is imposed as a boundary condition to Section 1:

$$\vec{V}_{i,1} = \vec{V}_{i,2} - (U_{\mathrm{b},1} - U_{\mathrm{b},2})\hat{n}_1. \tag{4}$$

Here index i loops over the control surfaces at Section 1 and their counterparts at Section 2, subscripts 1 and 2 indicate the section, $\hat{n}$ is the unit normal vector pointing outward from the surface of the section (see Fig. 2), $U_{\mathrm{b},1}$ is the bulk inflow velocity that satisfies the mass flow rate and $U_{\mathrm{b},2}$ is the bulk velocity at Section 2 calculated at the end of each non-linear iteration using the relation:

$$U_{\mathrm{b},2} = \frac{\int_{A_2} \rho \vec{V} \cdot \hat{n}\,\mathrm{d}s}{\int_{A_2} \rho\,\mathrm{d}s}, \tag{5}$$

where A_2 is the area of Section 2. In this manner, the mass is conserved with a minimum of induced error. Note that the correction term $(U_{\mathrm{b},1} - U_{\mathrm{b},2})$ approaches zero as the flow converges to its fully developed state.

A zero-gradient condition is the most commonly used condition for the outlet boundary, however, the periodicity of the flow structure suggests that the velocity gradients at Section 3 must be equal to the velocity gradients at Section 2, that is to say

$$\nabla \vec{V}_{i,3} = \nabla \vec{V}_{i,2}, \tag{6}$$

where index i loops over the control surfaces at Section 3 and their counterparts at Section 2 and subscripts 3 and 2 indicate the section. This condition generates less restriction and hence the boundary is more transparent to the computational domain.

Using this mass flow-based condition, momentum is conserved by allowing the pressure field to evolve, however pressure conditions must be imposed that ensure the correct pressure field. A reference (zero) pressure level is defined at the outlet boundary. The shape of the outlet pressure profile is obtained from Section 2 and is adjusted using the following relation to generate zero pressure force:

$$P_{i,3} = P_{i,2} - P_{\mathrm{a},2}, \tag{7}$$

where $P_{\mathrm{a},2}$ is the average pressure at Section 2 and is calculated at the end of each non-linear iteration using

$$P_{\mathrm{a},2} = \frac{\int_{A_2} P\,\mathrm{d}s}{\int_{A_2} \mathrm{d}s}. \tag{8}$$

The adjusted pressure profile is imposed node-by-node to Section 3 as a boundary condition. At the inlet, the pressure is extrapolated from inside the domain. Eqs. (4)–(8) form a well-posed set of boundary conditions that capture the periodicity of the flow in the computational domain.

3.2. Thermal periodic boundary condition

In a fully developed temperature field, the convective heat transfer coefficient h is solely a function of the flow structure. Therefore, for fully developed flow in a periodic geometry, h is identical for each consecutive periodic cross-section. That is, for the three sections shown in Fig. 3

$$h_1 = h_2 = h_3. \tag{9}$$

The cell-based average convective heat transfer coefficient $\bar{h}_{\mathrm{c}}$, which is defined as

$$\bar{h}_{\mathrm{c}} = \frac{\int_{A_{\mathrm{w,c}}} h\,\mathrm{d}A_{\mathrm{w}}}{A_{\mathrm{w,c}}} \tag{10}$$

is also identical for each cell. Here, $A_{\mathrm{w,c}}$ is the total wall area of a cell and $\mathrm{d}A_{\mathrm{w}}$ is its differential.

Two types of wall heating are considered herein, namely, heat transfer from a wall with constant temperature and heat transfer from a wall with a constant heat flux. In both cases, the fully developed temperature field continuously varies in the streamwise direction. Therefore, to observe a section of a fully developed flow and study the heat transfer process, it is necessary to prescribe the inflow bulk temperature. The bulk temperature at a section normal to the streamwise direction is defined in the following. For the differential control volume shown in Fig. 3 (assuming constant specific heat) the conservation of energy can be simplified to

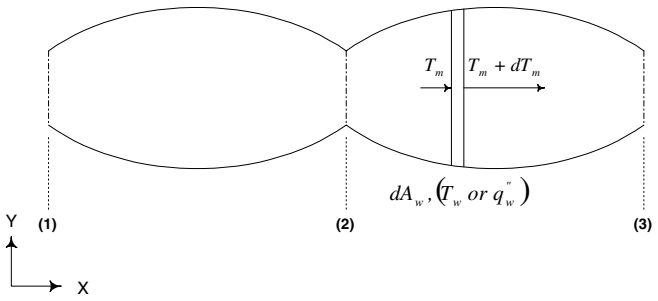

Fig. 3. Schematic showing a differential control volume of the double-periodic-cell and the details of heat convection process.

$$\dot{m}c_p\,\mathrm{d}T_\mathrm{b} = \ddot{q}_\mathrm{w}\,\mathrm{d}A_\mathrm{w}, \tag{11}$$

where $\dot{m}$ is the mass flow rate, $\ddot{q}$ is the wall heat flux per unit area and T_b is the bulk or mixing-cup temperature, which is defined as

$$T_\mathrm{b} = \frac{\int_A (T)\rho\vec{V}\cdot\hat{n}\,\mathrm{d}s}{\int_A \rho\vec{V}\cdot\hat{n}\,\mathrm{d}s} \tag{12}$$

for a section A normal to the streamwise direction.

For constant wall temperature, $\ddot{q}_\mathrm{w}$ is not constant. However, Eq. (11) can be re-written in the form of

$$-\dot{m}c_p\,\mathrm{d}(T_\mathrm{w} - T_\mathrm{b}) = h(T_\mathrm{w} - T_\mathrm{b})\,\mathrm{d}A_\mathrm{w} \tag{13}$$

and therefore,

$$\left(\frac{T_\mathrm{w} - T_\mathrm{b,out}}{T_\mathrm{w} - T_\mathrm{b,in}}\right)_\mathrm{c} = \exp\left(-\frac{A_\mathrm{w,c}}{\dot{m}c_p}\bar{h}_\mathrm{c}\right), \tag{14}$$

where $T_\mathrm{b,in}$ and $T_\mathrm{b,out}$ are the inflow and outflow bulk temperatures of a cell, respectively, and subscript c indicates cell-based values. For a periodic flow where $\dot{m}$, $A_\mathrm{w,c}$ and $\bar{h}_\mathrm{c}$ are constant, this ratio is a constant that characterizes the similarity of the thermal process in each cell. If we refer to this ratio as *logarithmic heat ratio*, r_h, then

$$T_\mathrm{b,in} = T_\mathrm{w} - r_\mathrm{h}^{-1}(T_\mathrm{w} - T_\mathrm{b,out}). \tag{15}$$

Thus, the relation

$$T_{i,1} = T_\mathrm{w} - r_\mathrm{h}^{-1}(T_\mathrm{w} - T_{i,2}) \tag{16}$$

can be used as a general expression for transferring information from Section 2 to Section 1. Here, index i loops over the control surfaces at Section 1 and their counterparts at Section 2, subscripts 1 and 2 indicate the section and

$$r_\mathrm{h} = \frac{T_\mathrm{w} - T_\mathrm{b,2}}{T_\mathrm{w} - T_\mathrm{b,1}} \tag{17}$$

is calculated at the end of each non-linear iteration and is converged to its accurate value when the solution is converged. Eq. (16) is a relative scaling formula that is used to specify an inlet temperature profile that is similar to the temperature profile at Section 2, but scaled using the wall temperature, T_w, and bulk inflow temperature, $T_\mathrm{b,1}$.

For the case of a constant wall heat flux, integrating Eq. (11) over a periodic cell leads to

$$(T_\mathrm{b,out} - T_\mathrm{b,in})_\mathrm{c} = \frac{\ddot{q}_\mathrm{w}}{\dot{m}c_p}A_\mathrm{w,c}. \tag{18}$$

Moreover, for a constant wall heat flux, from Eq. (9) it is expected that

$$T_\mathrm{w} - T_\mathrm{b,1} = T_\mathrm{w} - T_\mathrm{b,2} = T_\mathrm{w} - T_\mathrm{b,3}. \tag{19}$$

This suggests that the shape of the temperature profile does not vary for periodic sections and hence, a method similar to that implemented for the inlet velocity profile can be adopted for the inlet temperature profile. However, to form a consistent method for both wall boundary types, a scaling formula similar to Eq. (16) is used here, i.e. for a fixed bulk inflow temperature $T_\mathrm{b,1}$

$$T_{i,1} = T_\mathrm{ref} - r_\mathrm{c}^{-1}(T_\mathrm{ref} - T_{i,2}), \tag{20}$$

where T_ref is a reference temperature that can be assumed as $T_\mathrm{ref} = 0$ and r_c is a cell-based heat ratio similar to the logarithmic heat ratio, which is calculated at the end of each iteration using the formula:

$$r_\mathrm{c} = \frac{T_\mathrm{ref} - T_\mathrm{b,2}}{T_\mathrm{ref} - T_\mathrm{b,1}}. \tag{21}$$

It is clear that the value of r_c is different for each cell and approaches one asymptotically as cells further downstream are considered.

While the gradient of temperature at Section 3 is equal to that at Section 2 for a constant wall heat flux, it is not the case when the wall temperature is constant. Moreover, a zero gradient is also not physically realistic at the outlet boundary. Therefore, to improve the approximation at Section 3, the gradient of temperature for each node is extrapolated from the center of the nearest internal control volume.

Implementation of the proposed thermal periodic condition together with Eqs. (12), (16), (17), (20) and (21) forms a set of well-posed boundary conditions for all types of wall heating to simulate the periodicity in the heat transfer process. Compared to the thermal periodic conditions proposed by Patankar et al. (1977), the present method is more general in terms of the difference between isoflux and isothermal wall heating, requires less computational effort since no additional differential equations need to be solved, and is easier to implement since information is only required at three spatially periodic sections of the domain. As such, the proposed condition can be used with structured and unstructured grids and can be readily implemented in existing CFD codes.

4. Validation

The pressure drop and heat transfer for two different periodic geometries are considered to validate the thermal periodic boundary condition proposed herein: a pipe with a unit diameter and an idealized porous media with an interconnected spherical pore structure. A no-slip boundary condition was imposed at the walls and the periodic boundary conditions described above are implemented at the inlet and outlet. The linear system of equations is normalized by the diagonal elements and the non-linear convergence criteria is set to 10^{-4} with a maximum of 10 non-linear iterations per time-step. The steady state results for all test cases are obtained for a maximum steady state error of 10^{-5}. All simulations were performed using a distributed-memory cluster of 16 Compaq Alpha processors with a processor speed of 533 MHZ and a memory of 1 GB per processor. This cluster is provided by SHARCNET (2006).

4.1. Case 1: Circular pipe, constant heat flux

Laminar flow in a circular pipe with a constant wall heat flux is considered. Among the three test cases described herein, this is the most straightforward case because the shape of the temperature profile is similar for all axial cross-sections and the accuracy of the method is not influenced by the flow Peclet number. As such, only two different Peclet numbers are considered. Flow Reynolds numbers of $Re = \rho U_{b,1} D/\mu = 10$ and 100 with a constant wall heat flux of $\ddot{q}_w = 200\ \mathrm{W/m^2}$ were simulated for a fluid with $\rho = 1.0$, $\mu = 0.1$ and $k = 1.0$ and Prandtl number $Pr = 1.0$. The circular-pipe domain was arbitrarily chosen to be a unit diameter ($D = 1.0$) and five units in length. As such, each periodic cell of the double-periodic-cell domain is one unit in diameter ($D = 1.0$) and 2.5 units in length. The three-dimensional domain was discretized into 17,550 hexahedral control volumes. Fig. 4 shows an overall picture of the grid. Control-volumes were concentrated towards the pipe wall and the periodic sections; the grid size in the streamwise direction near Sections 1–3 is approximately $0.07D$.

The analytical solutions for the fully developed flow and temperature field of this condition are obtained from Incropera and DeWitt (2002): the pressure drop for fully developed flow in a pipe with a diameter of D and length L is

$$\Delta P = -\frac{32\mu}{D^2} U_{b,1} L, \tag{22}$$

where $U_{b,1}$ is the bulk inlet velocity, and the Nusselt number for fully developed flow with a constant heat flux condition is $Nu = 4.36$.

The computed velocity profiles and pressure drop were within 0.25% of the analytical solution for both Reynolds numbers considered, thereby validating the implementation and accuracy of the flow periodic condition. The Nusselt number is calculated at each section using

$$Nu = \frac{hk}{D}, \quad \text{where } h = \frac{\ddot{q}_w}{T_w - T_b}. \tag{23}$$

The Nusselt numbers computed for the inlet, middle section and outlet of the double-periodic-cell are 4.25, 4.35, and 4.35, respectively, for $Re = 10$ ($Pe = 10$) and 4.25, 4.35 and 4.35, respectively, for $Re = 100$ ($Pe = 100$). The results confirm that the proposed condition yields predictions of the Nusselt number that are axially constant and within 3% of the analytical value for both Reynolds numbers considered. Temperature contours are shown in Fig. 5. The figure confirms that the computed temperature contours are similar over the entire computational domain.

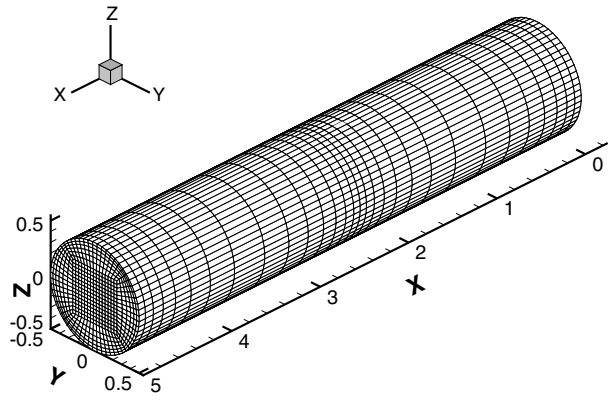

Fig. 4. A grid of 17,550 control-volumes forming a double-periodic-cell of a circular pipe.

4.2. Case 2: Circular pipe, constant wall temperature

The geometry and grid used in this test are the same as those described for test case 1. For the case of constant wall temperature in a fully developed circular pipe flow, the Nusselt number has a constant value of $Nu = 3.66$ (Incropera and DeWitt, 2002). In this case, the shape of the temperature profile varies axially and the accuracy of the simulation depends highly on the accuracy of the prediction of the inflow temperature profile. Recall that the inflow temperature profile is predicted in each non-linear iteration by extrapolating the temperature profile from the middle-section (Section 2) using Eq. (16). Since for low Peclet numbers ($Pe = Re \times Pr$), the temperature profile further downstream asymptotically flattens, it is important to verify the accuracy of the method for a wide range of Peclet numbers and temperature differences. To this end, a range of test cases with different Reynolds numbers, Prandtl numbers and wall temperatures are presented. Table 1 summarizes the conditions considered and the results of the test cases. The Nusselt number for each periodic cell is calculated using Eqs. (A.4) and (A.8), which are described in Appendix A. It is shown in Table 1 that the maximum error occurs for the case of $Pe = 25$ and is less than 1.5%. The accurate prediction of the Nusselt number even for low Peclet numbers confirms the accuracy of the extrapolation method used in the present method. Comparison of Cases 2b and 2c shows that the inflow-to-wall temperature difference also has no significant effect on the accuracy of the method. The asymptotic behavior of the temperature in the streamwise direction can be observed in Fig. 6 where the temperature variation along the streamwise centerline for Case 2a is shown. Fig. 7 shows temperature profiles at the inlet, middle section and outlet of the domain for Case 2a ($Pe = 25$). The significant change in the shape of the temperature profiles at the periodic cross-sections can be observed in this figure. Fig. 8 shows temperature contours for Case 2b, where the development of the entire temperature field is illustrated.

4.3. Case 3: Idealized porous media

As a final validation of the proposed thermal periodic boundary condition, the case of convective heat transfer in an idealized porous material is simulated. The material considered has a highly porous, interconnected spherical void structure and is characterized using the unit-cube geometry model proposed by Yu et al. (2006). Fig. 9(a)

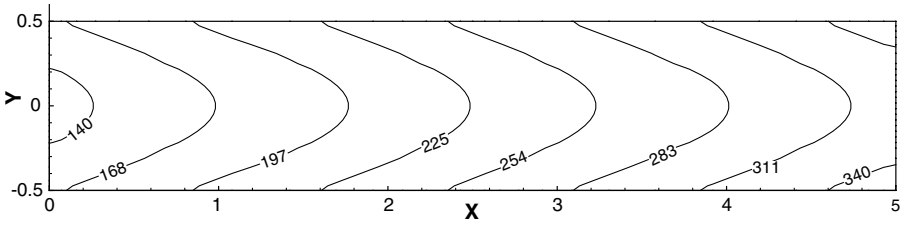

Fig. 5. Temperature contours for the case of constant wall heat flux (Case 1).

Table 1
Nusselt number for a circular pipe flow with constant wall temperature

Case	Pe	$T_w - T_{b,1}$	Nu	Error (%)
a	25	200	3.61	1.3
b	100	50	3.67	<1
c	100	200	3.67	<1
d	500	200	3.67	<1
e	2000	200	3.67	<1

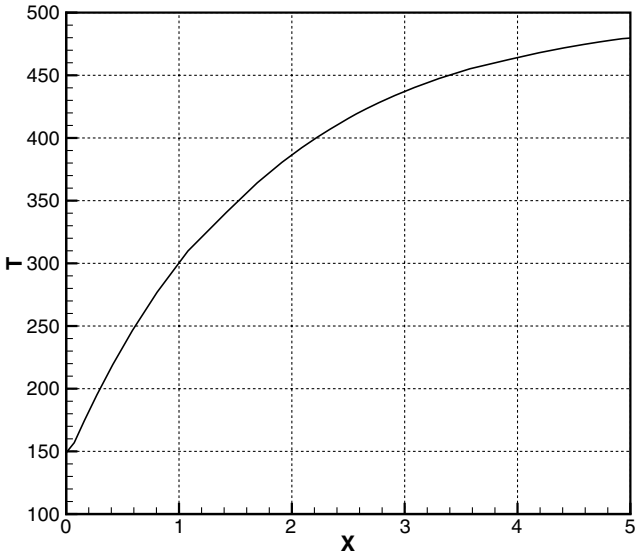

Fig. 6. Temperature profile along the streamwise centerline (Case 2a).

shows the idealized geometry. The unit-cube geometry is characterized by the pore diameter (D_p) and the porosity (ϵ) of the porous material being considered. The size of the unit-cube (H) and the pore window diameter (d) are defined by the given pore diameter and porosity.

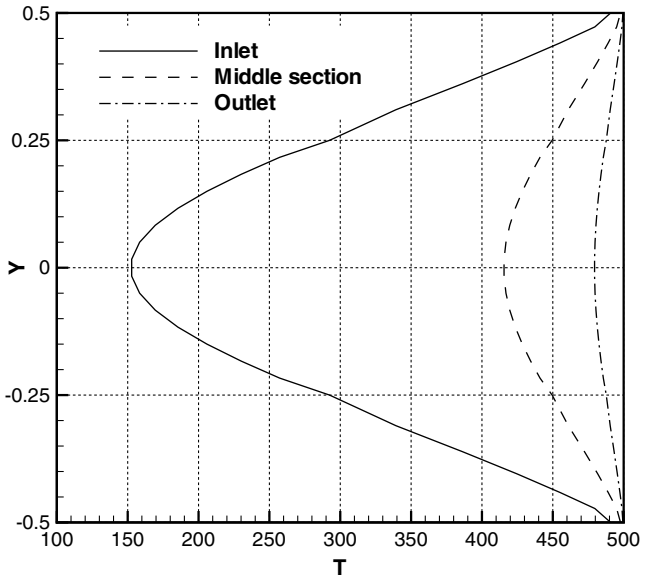

Fig. 7. Temperature profile at the three periodic sections of the domain (Case 2a).

A unit-cube model is generated to compute the hydraulic and thermal characteristics of a porous material with a porosity of $\epsilon = 0.80$ and pore diameter of $D_p = 450$ μm, for which, the unit-cube size is $H = 374$ μm. The computational domain is reduced to a quarter of the physical domain by the virtue of symmetry of the flow field. A double-periodic-cell geometry is generated for this geometry. Fig. 9(b) illustrates an outline of the double-periodic-cell. Fully developed steady laminar thermo-fluid flow with a constant wall temperature is simulated for a range of pore-level Reynolds numbers (Re_D). The maximum pore-level Reynolds number for this regime is $Re_D = V_{int} D_p/\nu = 150$ (Pedras and de Lemos, 2001), where V_{int} is the intrinsic velocity. The actual pore-window mean velocity,

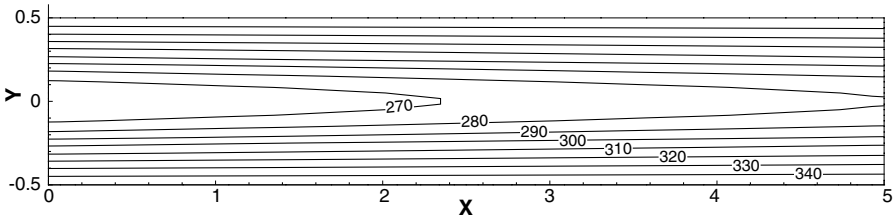

Fig. 8. Temperature contours for the case of constant wall temperature (Case 2b).

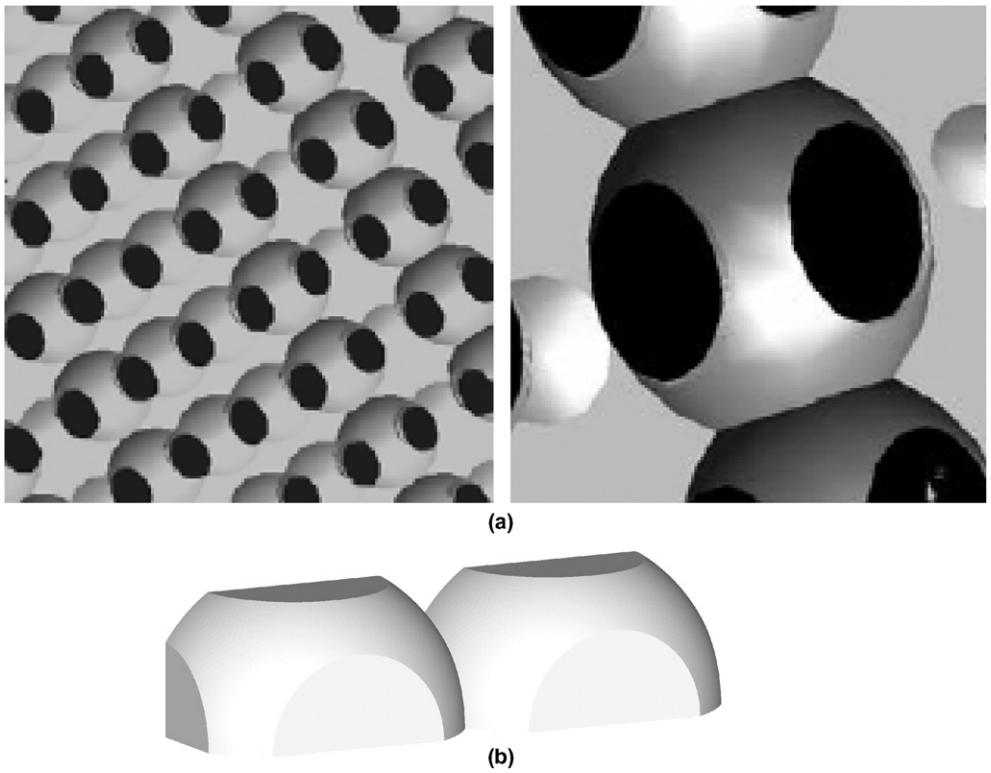

Fig. 9. (a) Internal structure (left) and a single pore (right) of the idealized porous material; (b) The computational domain for a double-periodic-cell based on a quarter of the unit-cube model of an idealized porous material with $\epsilon = 0.80$ and $D_p = 450$ μm ($H = 374$ μm).

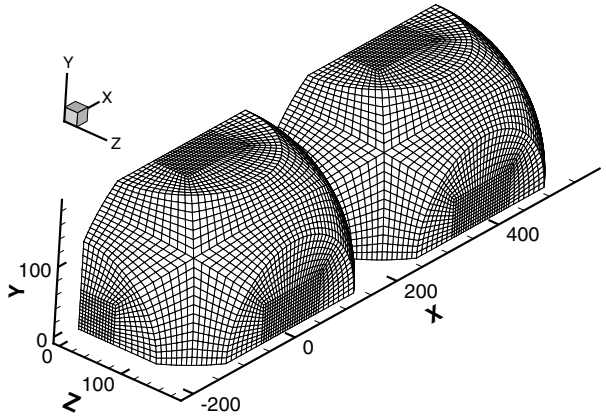

Fig. 10. An outline of Grid 3 with 84,960 control volumes and near-wall grid size of $\Delta_w = 4$ μm.

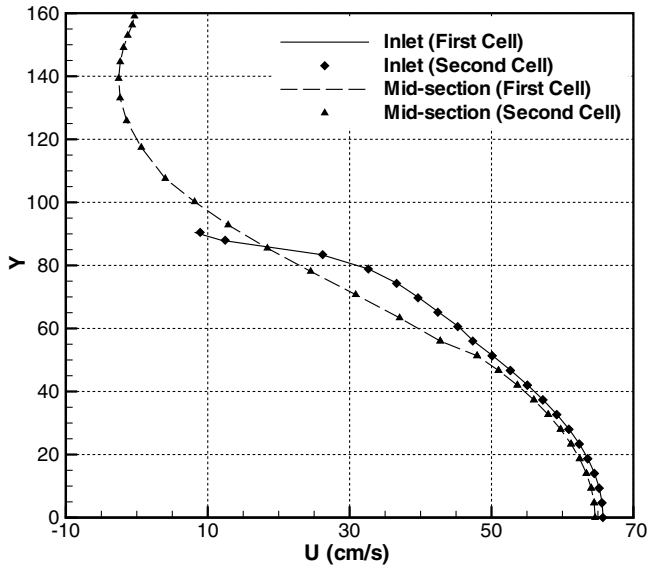

Fig. 11. Comparison of the velocity profiles at cross-sections located at the inlet and middle of each cell.

from which the inlet mass-flow rate is specified, is calculated using

$$U_{b,1} = \frac{4H^2}{\pi d^2} V_{ext}, \tag{24}$$

where V_{ext} is the extrinsic velocity, $V_{ext} = \epsilon V_{int}$.

Symmetry boundary conditions are imposed at the symmetry planes. A no-slip boundary condition is imposed at the walls and the proposed periodic boundary condition model is implemented at the periodic sections.

To ensure grid independent simulations, a grid convergence study is performed. Four grids with wall-grid size of $\Delta_w = 9$ μm for Grid 1 with 11,000 control volumes, $\Delta_w = 6$ μm for Grid 2 with 26,816 control volumes, $\Delta_w = 4$ μm for Grid 3 with 84,960 control volumes and $\Delta_w = 3$ μm for Grid 4 with 187,207 control volumes are generated. Fig. 10 shows an outline of Grid 3. Flows with Reynolds numbers of $Re_D = 40$ and $Re_D = 100$ are simulated. Water with $Pr = 5.854$ at the bulk temperature of

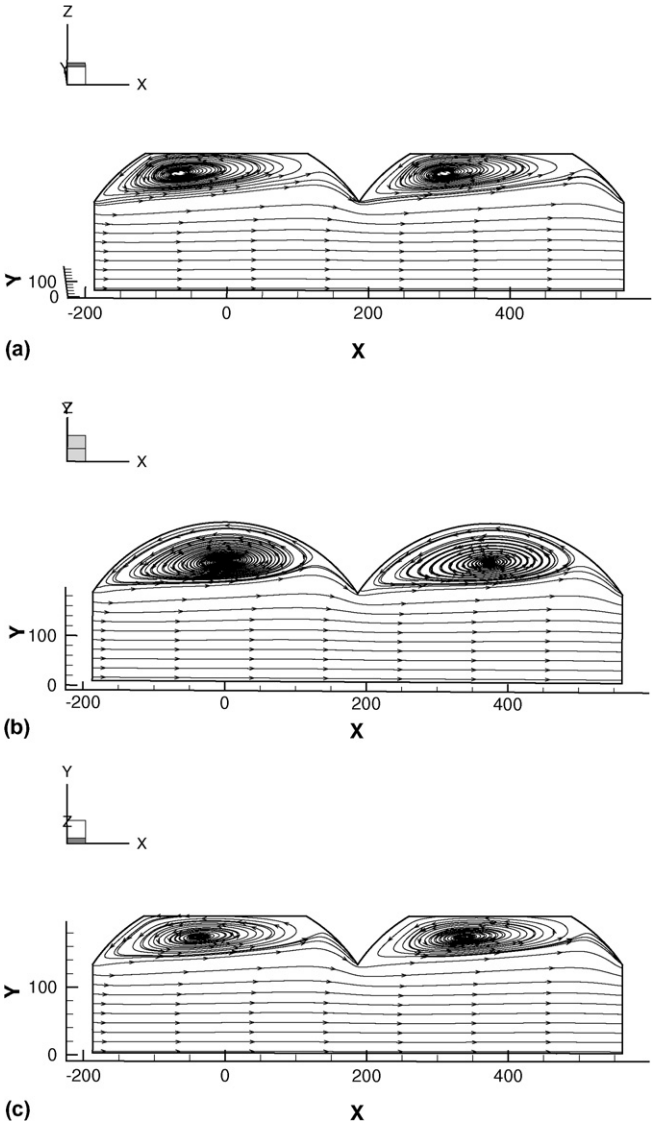

Fig. 12. Streamlines at (a) a cross-section 15° from zx-symmetry plane, (b) a cross-section 45° from zx-symmetry plane and (c) a cross-section 75° from zx-symmetry plane for the case of $Re_D = 100$.

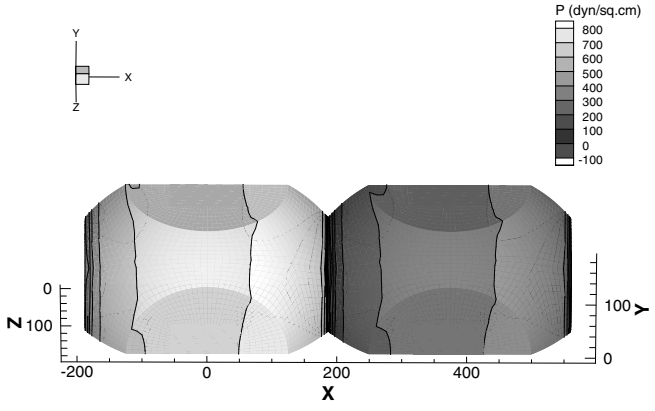

Fig. 13. Pressure contours for $Re_D = 100$.

$T_{b,1} = 300$ K enters the flow field, while a constant wall temperature of $T_w = 350$ K is imposed. Fig. 11 compares the velocity profiles at the inlet and middle of the first periodic cell to those located at the inlet and middle of the second periodic cell, respectively, to confirm the accuracy of the flow periodic boundary conditions. Fig. 12 shows streamlines in three streamwise cross-sections for the case of $Re_D = 100$. The size of the separation zones in two

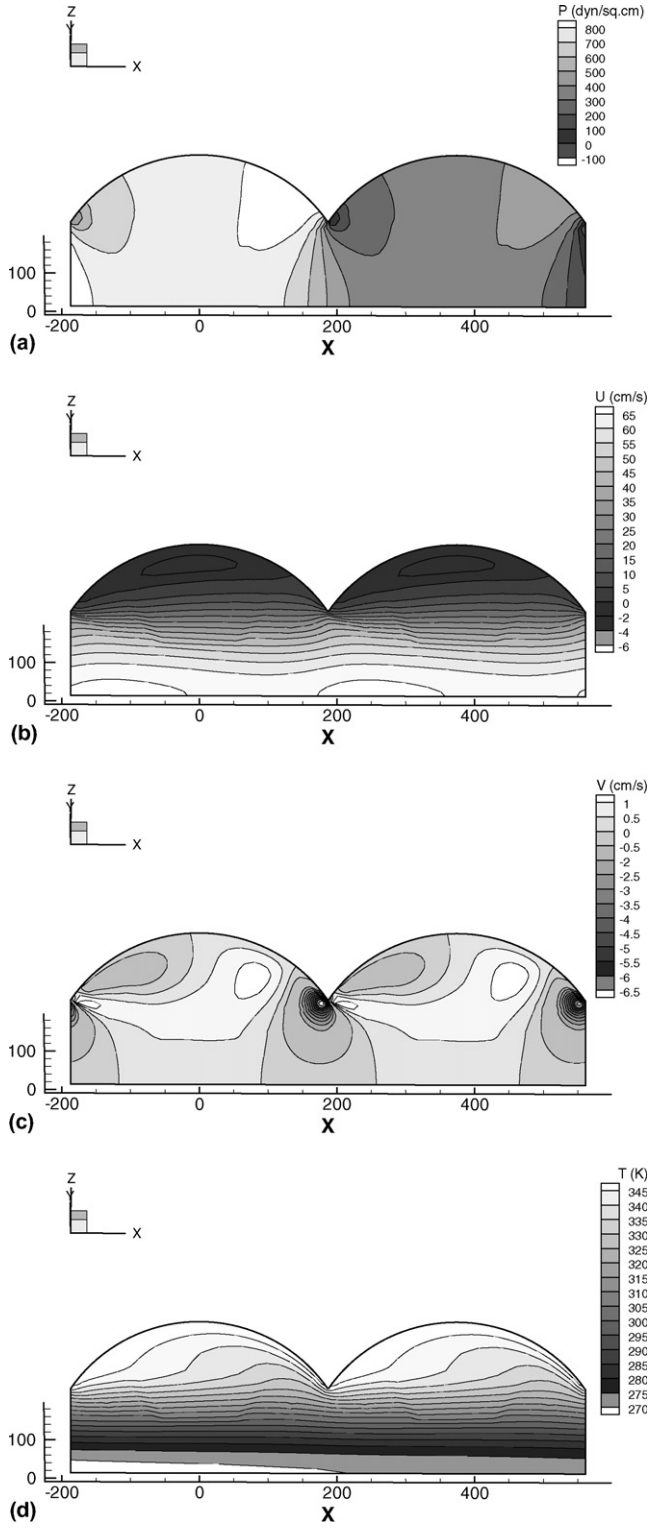

Fig. 14. Contours for (a) pressure, (b) U-velocity, (c) V-velocity and (d) temperature at a cross-section between two symmetry planes (45° from zx-symmetry plane), $Re_D = 100$.

Table 2
Nusselt number and pressure drop for different grids (idealized porous media)

Re_D	Grid	$\frac{\Delta P}{\mu U_{b,1}/D_p}$	$\delta(\Delta P)$, %	Nu_D	$\delta(Nu_D)$, %
40	1	39.6		5.024	
	2	40.3	1.7	5.067	<1
	3	41.0	1.7	5.073	<1
	4	41.5	1.2	5.073	0.0
100	1	47.1		5.385	
	2	48.0	1.9	5.346	<1
	3	48.3	<1	5.301	<1
	4	48.7	<1	5.281	<1

consecutive cells are identical, illustrating the periodicity of the flow field. Fig. 13 shows pressure contours for the case of $Re_D = 100$. The overall similarity of the pressure field in the two cells can be observed in this figure. Fig. 14 shows contours of independent flow and temperature variables at a cross-section between two symmetry planes for a flow with $Re_D = 100$. The periodicity of the flow and temperature field can be clearly observed in this figure. There is no significant disturbance in the contour lines crossing the outlet and inlet of the computational domain. This can be seen more clearly in Fig. 14(b) and (d). The resemblance of the contour lines crossing the domain inlet and outlet boundaries with those crossing the mid-section proves that the outlet and inlet boundaries are essentially transparent to the flow and temperature field. According to Table 2, which summarizes the grid convergence study, the results of the computation for Grid 3 are independent of the mesh size and thus is selected as a grid for further test cases. In this table, Nu_D is the pore-level Nusselt number that is computed for one unit-cube cell using Eqs. (A.4) and (A.8), where the length-scale D is replaced by the pore diameter D_p. It is worth mentioning here that the difference between the pressure drop of the first cell and the second cell did not exceed 4% and the difference between the Nusselt number of two consecutive cells was less than 1%. Again, the grid-converged results demonstrate the accuracy of the proposed thermal periodic boundary condition.

5. Conclusion

A periodic boundary condition is proposed to predict heat transfer in spatially periodic flows. The condition is formulated to be used in a double-periodic-cell domain in conjunction with the mass-based condition developed by El Soukkary and Straatman (2003). The condition is consistent for both isothermal and isoflux wall thermal conditions; it does not require any modification to the energy equation and does not require solution of any additional partial differential equations. The fully developed temperature field is predicted using this condition by scaling the information from the mid-section of the domain using a physically reasoned logarithmic scaling law and imposing at the inlet section and requires no additional information from inside the computational domain and thus suitable for both structured and unstructured grids. The condition was validated by presenting simulations of the flow in circular pipes with constant heat flux and constant wall temperature and an idealized spherical void phase porous material. The non-linear convergence of all simulations were smooth and monotonic. The pipeflow cases were within 1% of the analytical result, while the remaining cases yielded the correct physical trends, thereby confirming the utility of the boundary condition.

Acknowledgments

The authors gratefully acknowledge the financial support from the Natural Science and Engineering Research Council (NSERC) and from SHARCNET.

Appendix A. Processing of results

From Eqs. (18) and (14), the total convective heat transfer in a single cell with a constant wall temperature of T_w can be calculated as

$$q_c = \bar{h}_c A_{w,c} \Delta T_{lm}, \tag{A.1}$$

where ΔT_{lm} is the log-mean temperature difference,

$$\Delta T_{lm} = \frac{(T_{b,in} - T_{b,out})_{cell}}{\ln(r_h)}. \tag{A.2}$$

To obtain the Nusselt number for a periodic cell of a periodic geometry with constant wall temperature from the steady state results, the bulk temperature at each section is calculated and the total heat transfer is obtained as

$$q_c = \dot{m} c_p (T_{b,out} - T_{b,in})_c. \tag{A.3}$$

The cell-based average convective heat transfer coefficient is then obtained as

$$\bar{h}_c = \frac{q_c}{A_{w,c} \Delta T_{lm}}. \tag{A.4}$$

In the case of a constant heat flux of $\ddot{q}_w$, the cell-based average convective heat transfer is calculated using relation:

$$\bar{h}_c = \frac{\ddot{q}_w}{\overline{T}_{w,c} - \overline{T}_{b,c}}, \tag{A.5}$$

where $\overline{T}_{w,c}$ is cell-based average wall temperature,

$$\overline{T}_{w,c} = \frac{\int_{A_{w,c}} T_w \, dA_w}{A_{w,c}} \tag{A.6}$$

and $\overline{T}_{b,c}$, cell-based average bulk temperature, is calculated using formula:

$$\overline{T}_{b,c} = \frac{\int_{V_c} \rho T \vec{V} \cdot \hat{n} \, dv}{\int_{V_c} \rho \vec{V} \cdot \hat{n} \, dv}. \tag{A.7}$$

Here, V_c is the volume of a cell, dv is the volume differential and $\hat{n}$ is a unit vector normal to the periodic sections (streamwise direction normal vector).

The cell-based Nusselt number is defined as

$$\overline{Nu} = \frac{\bar{h}_c D}{k}, \tag{A.8}$$

where D is a proper length scale related to the size of the periodic cell. It is expected that $\overline{Nu}$ is constant for a periodic geometry. Therefore, comparing $\overline{Nu}_1$ and $\overline{Nu}_2$ – the cell-based Nusselt number for two consecutive cells – can be considered a measure of the accuracy and validation of the method.

References

Balay, S., Buschelman, K., Gropp, W.D., Kaushik, D., Knepley, M.G., McInnes, L.C., Smith, B.F., Zhang, H., 2001. PETSc Homepage. URL: http://www.mcs.anl.gov/petsc.

El Soukkary, T., Straatman, A.G., 2003. The prediction of spatially periodic flows using a finite-volume model. International Journal for Numerical Methods in Fluids 41, 303–317.

Incropera, F.P., DeWitt, D.P., 2002. Fundamentals of Heat and Mass Transfer, fifth ed. John Wiley & Sons.

Karimian, S.A.M., Straatman, A.G. Discretization and parallel performance of an unstructured finite volume Navier–Stokes solver. International Journal for Numerical Methods in Fluids, in press, doi:10.1002/fld.1189.

Kholsa, P., Rubin, S., 1974. A diagonally dominant second-order accurate implicit scheme. Computers and Fluids 2, 207–209.

Nicolas, X., Traore, P., Mojtabi, A., Caltagirone, J.P., 1997. Augmented Lagrangian method and open boundary conditions in 2D simulation of Poiseuille–Bénard channel flow. International Journal for Numerical Methods in Fluids 25, 265–283.

Orlandi, P., 2000. Fluid Flow Phenomena: A Numerical Toolkit. Kluwer, Dordrecht, Boston.

Patankar, S.V., Liu, C.H., Sparrow, E.M., 1977. Fully developed flow and heat transfer in ducts having streamwise-periodic variations of cross-sectional area. Journal of Heat Transfer – Transactions of the ASME 99, 180–186.

Pedras, M.H., de Lemos, M.J., 2001. Macroscopic turbulence modeling for incompressible flow through undeformable porous media. International Journal of Heat and Mass Transfer 44, 1081–1093.

SHARCNET, 2006. Sharcnet homepage. URL: http://www.sharcnet.ca.

Yu, Q., Thompson, B.E., Straatman, A.G., 2006. A unit cube-based model for heat transfer and fluid flow in porous carbon foam. ASME Journal of Heat Transfer 128, 352–360.